

Effects of Magnetic Shielding Configuration on Discharge Characteristics and Performance of a 60 mm-Diameter Low-Power Hall Thruster

Weilong Guo^{1,*} , Jun Gao¹ , Zuo Gu¹ , Ning Guo¹ , Ming-ming Sun¹ 

¹China Academy of Space Technology – Lanzhou Institute of Physics – Science and Technology on Vacuum Technology and Physics Laboratory – Lanzhou/Gansu – China.

*Corresponding author: 1347458669@qq.com

ABSTRACT

Lifetime is a main factor restraining the application of low-power Hall thruster. Magnetic shielding configuration is regarded as a promising method to prolong the lifespan of Hall thruster. Aiming to demonstrate the feasibility and effectiveness of magnetic shielding configuration applying on low-power Hall thruster, a 60-mm diameter Hall thruster in partial magnetic shielding configuration was designated. Both the numerical and experimental methods were used to investigate the discharge characteristics of the Hall thruster and help understand the mechanism behind. The maximum anode efficiency was achieved as high as 29.7% with $1.7 \text{ mg}\cdot\text{s}^{-1}$ anode mass flow and 320 V discharge voltage. To evaluate the effectiveness of the magnetic shielding used for low-power Hall thruster, a 2000 h lifetime test has been carried out and the results indicate that the erosion rate has been decreased below $0.2 \mu\text{m}\cdot\text{h}^{-1}$.

Keywords: Hall thruster; Magnetic shielding; Performance; Lifetime Test.

INTRODUCTION

For the past few years, the new aerospace applications represented by microsatellite network promote the development of the low-power Hall thruster ($< 500 \text{ W}$ and $< 7 \text{ cm}$ diameter) (Grimaud and Mazouffre 2017). Numerous high special impulse low-power Hall thrusters have been developed, and some of them have been applied in orbit successfully. Meanwhile, lifetime is still a restriction for use of the low-power Hall thruster (Conversano *et al.* 2015; Mikellides and Hofer 2013).

The BHT-200 operates at 11.4 mN under 200 W, while having an operational life no longer than 1000 h (Hargus Junior and Charles 2003). The SPT-30, which is a 30-mm diameter Hall thruster, could produce a thrust of 11.3 mN with the anode efficiency of 32%, but its lifetime is approximately 600 h (Hruby *et al.* 1999; Jacobson and Jankovsky 1998).

Generally, the primary factor that restricts the lifetime of the Hall thruster is the erosion of the discharge channel walls caused by ion bombardment, from which the low-power Hall thrusters will suffer more severely for its inherently larger surface-to-volume ratios (Conversano *et al.* 2015).

Received: Jan. 22, 2021 | Accepted: Apr. 13, 2021

Peer Review History: Single Blind Peer Review.

Section Editor: José A Fritz F Rocco



This is an open access article distributed under the terms of the Creative Commons license.

Application of magnetic shielding in Hall thruster effectively restrains the erosion of the discharge channel, and then prolongs the thruster lifetime. Since the magnetic shielding effect was discovered in BPT-4000 (Mikellides *et al.* 2010; 2011), a 4000-W Hall thruster designed for geosynchronous orbit (GEO) satellite, some thrusters in medium power (1 ~ 10 kW), or higher (> 10 kW) have succeeded in employing this new magnetic configuration to reduce erosion of the wall. The magnetic shielding technique has been regarded as a promising method to prolong the lifetime of the Hall thruster.

However, the inherent problems of the low-power Hall thruster, such as insufficient room for magnetic components and so on, make it a challenging prospect to apply magnetic shielding to low-power Hall thruster. Researches have been conducted on this prospect.

Grimaud designed a 200-W Hall thruster under magnetic configuration called ISCT200-Ms, producing 11.4 mN thrust and 920 s special impulse (Grimaud and Mazouffre 2018). Busek developed a 100-W magnetic shielding Hall thruster, which has a performance of 6.57 mN and 1010 s special impulse (Szabo *et al.* 2017). Expect for the feasibility of the magnetic shielding configuration, low efficiency was measured in these thrusters. And all of these thrusters have not carried out a long-duration lifetime test.

Based on predecessors' work, a 60-mm diameter Hall thruster in magnetic configuration is designed, named LHT-60M, which has the same size as its unshielded counterpart, the LHT-60 thruster. The LHT-60M thruster adopted partial magnetic shielding configuration and maintained a satisfactory efficiency, as well as long lifetime expectancy. It is also the first self-excited low-power magnetic shielding Hall thruster to the authors' knowledge.

In this text, the characteristics of the LHT-60M are presented. Both the experimental and numerical methods are employed to help understand the physical mechanisms of magnetic shielding configuration, as well as the effects on the performance. The rest of this paper is organized as follows: the magnetic design of Hall thruster is presented first, and the physical model is established in fluid method to described the variation of physical parameters. Based on the model, the numerical results are presented and the discharge characteristics inside the discharge channel under two different magnetic configurations are also analyzed. And then the experiment results are demonstrated and compared with the numerical results, and the results of lifetime test are also analyzed. The conclusion is provided at last.

MAGNETIC DESIGN

Magnetic shielding

Compared with the conventional configuration, the magnetic field lines extend from the magnetic pole shoe towards the anode with larger convex curvature, through the accelerating area, approximately parallel to the discharge channel wall. And the magnetic field lines connecting the pole shoe do not intersect the discharge channel walls in the acceleration region. The comparison between the two topologies is shown in Fig. 1.

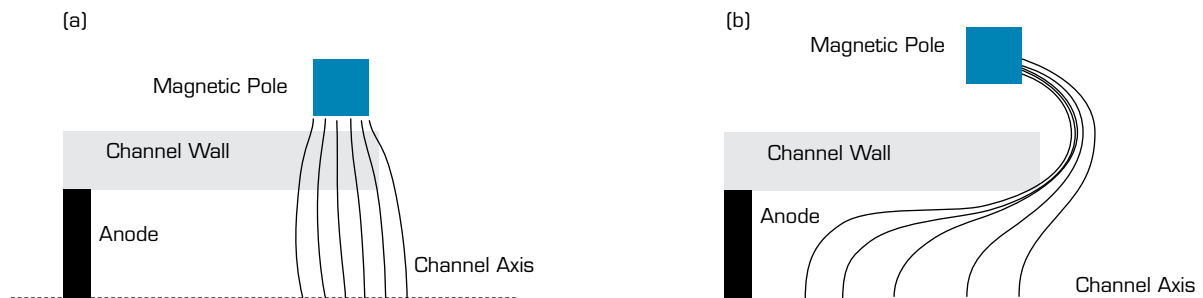


Figure 1. Comparison between conventional (a) and magnetic shielding (b) configuration.

The magnetic shielding topology could take full advantage of the isothermality of the magnetic field lines (Szabo *et al.* 2017), as shown in Eq. 1.

$$\nabla_{//} T_e = 0 \quad (1)$$

And the integral of the electric field along the magnetic field line from the centerline of the discharge channel can be expressed as Eq. 2, the thermalized potential equation, where Φ_0 and T_{e0} represent the plasma potential and the electron temperature in the centerline of the discharge channel, respectively (Szabo *et al.* 2017).

$$\Phi_T = \Phi_0 + T_{e0} \ln \left(\frac{n_{e0}}{n_e} \right) \quad (2)$$

Via magnetic field line extending to the anode, the electron temperature adjacent to the wall will be as low as that near the anode, and then $\Phi_T \approx \Phi_0$. The sheath potential accelerating ions toward the walls will be decreased.

Magnetic configuration and simulation region

To demonstrate the application and effectiveness of the magnetic shielding configuration on low-power Hall thruster, a 60-mm diameter Hall thruster called LHT-60M (Fig. 2) was designed based on its unshielded counterpart.



Figure 2. LHT-60M hall thruster.

A two-dimensional axisymmetric model is established to investigate the effects of different configurations. The simulation region is shown in Fig. 3a. The left side of the channel is the anode, which provides enough potential for ionization. And the right side is the free boundary where ions are ejected. The other boundaries are the wall of the channel, made of ceramic. The geometric dimensions of the discharge area have been normalized. In the following text, L represents the length of the discharge channel, z represents the axial position, H represents the width of the discharge channel, and h represents the radial position.

Giving that application of magnetic shielding configuration on low-power Hall thruster will decrease the efficiency, found in BHT-100 and ISCT200-Ms (Grimaud and Mazouffre 2018; Szabo *et al.* 2017), and the strict requirement for magnetic components, a partial magnetic shielding configuration was achieved, in which part of the magnetic lines were allowed to intersect the walls of acceleration region. The magnetic configurations of LHT-60 and LHT-60M are shown in Fig. 3a and Fig. 3b, respectively, and are called US configuration and MS configuration for short hereinafter.

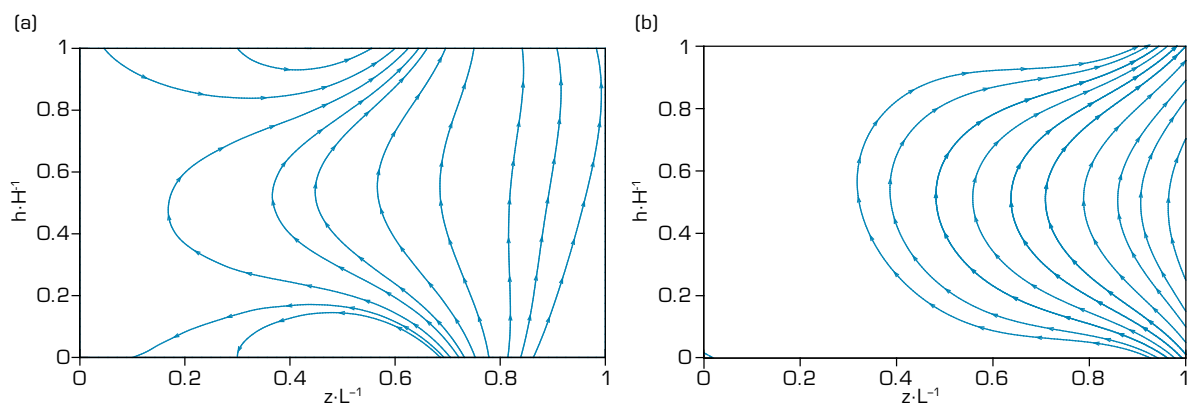


Figure 3. Magnetic configurations of LHT-60 and LHT-60M. (a) Unshielded (b) Magnetic shielding.

Figure 4 illustrates the radial magnetic flux density along the center line of the discharge channel of the two thrusters. Br is used to represent the radial magnetic flux density. It can be seen that the maximum value of Br in the MS configuration appears closer to the exit.

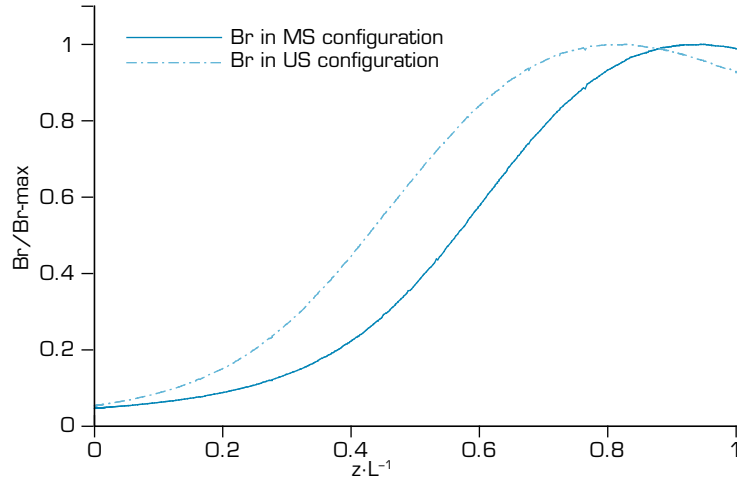


Figure 4. Magnetic flux density along the center line of the discharge channel.

PHYSICAL MODEL IN DISCHARGE CHANNEL

Spatial potential in discharge channel

The plasma potential can be resolved via Poisson's equation, which is obtained by Maxwell's equation, shown in Eq. 3, where Φ is used to denote the plasma potential, and n_i denotes the ion density, while n_e denotes the electron density correspondingly. The potential of the anode is set to discharge voltage, and that at the exit is set to 0 V (Duan *et al.* 2016).

$$-\nabla^2 \Phi = \frac{e}{\epsilon_0} (n_i - n_e) \quad (3)$$

As for 2D axial symmetry computational model, the physical quantity could be regarded as the function of the r and z . Poisson's equation is written in type of component as Eq. 4.

$$-\frac{1}{r} \frac{\partial \Phi}{\partial r} \left(r \frac{\partial \Phi}{\partial r} \right) - \frac{\partial^2 \Phi}{\partial z^2} = \frac{e}{\epsilon_0} (n_i - n_e) \quad (4)$$

And the electric field could be obtained by Eq. 5:

$$E = -\nabla \Phi \quad (5)$$

Plasma motions in discharge channel

Fluid method has been verified effective in simulating discharging of the Hall thruster (Escobar and Ahedo 2015). In order to describe the plasma characteristic in the discharge channel of the Hall thruster, the electrons population could be treated as inviscid fluid (Escobar and Ahedo 2015; Mikellides *et al.* 2011). Electrons motions in the discharge channel can be described through electron density and electron energy, which could be resolved via equation of electron continuity and conservation of electron capacity.

The electron continuity equation is given by Eq. 6 and the conservation of electron capacity equation is shown in Eq. 7 (Ahedo *et al.* 2000; Escobar and Ahedo 2015):

$$\frac{\partial}{\partial t}(n_e) - \nabla[V_e n_e + \mu_e T_e \cdot \nabla n_e] = R_e \quad (6)$$

$$\frac{\partial}{\partial t}\left(\frac{3}{2}n_e T_e\right) + \nabla \cdot \left(-\frac{5}{2}n_e T_e V_e - \frac{5}{2}n_e \mu_e T_e \nabla(T_e)\right) - en_e V_e E - T_e V_e \cdot \nabla n_e = R_{en} \quad (7)$$

where n_e denotes the electron density and V_e is the velocity of the electrons. Ω_e represents the electron mobility, which can be expressed as Eq. 8, where Ω_e is the electron hall correction, expressed in Eq. 9 (Goebel and Katz 2008):

$$\mu_e = \frac{e}{m_e \nu(1 + \Omega_e^2)} \quad (8)$$

$$\Omega_e^2 = \frac{eB}{mV_e} \quad (9)$$

where ν denotes the collision frequency (Book 1987; Katz *et al.* 2004) between electrons and the neutral atoms, as shown in Eq. 10:

$$\nu = \nu_{en} + \nu_{ei} \quad (10)$$

R_e and R_{en} can be expressed as Eq. 11 and Eq. 12, respectively, where k_j denotes the velocity of the reaction j and ε_j denotes the energy loss in the reaction:

$$R_e = \sum_{j=1}^M k_j n_n n_e \quad (11)$$

$$R_{en} = \sum_{j=1}^P k_j n_n n_e \cdot \varepsilon_j \quad (12)$$

Reaction velocity k_j could be obtained in Eq. 13, where $f(\varepsilon)$ is the electron energy distribution function, that obey Maxwell distribution (Goebel and Karts 2008):

$$k_j = \sqrt{\frac{2e}{m_e}} \cdot \int_0^\infty \varepsilon \sigma_j(\varepsilon) f(\varepsilon) d\varepsilon \quad (13)$$

The transport process of particles except electrons could be described in Eq. 14, where J_k denotes the diffusion flux of particles k , and R_k represents the production rate of it. J_k can be obtained in Eq. 15, w_k is the quality fraction of particles k (Christou and Jugroot 2017; Goebel and Karts 2008):

$$\rho \frac{\partial}{\partial t}(w_k) + \rho(u \cdot \nabla) = \nabla J_k + R_k \quad (14)$$

$$J_k = \rho w_k V_k \quad (15)$$

And V_k denotes the diffusion velocity of particles k , which is shown in Eq. 16:

$$V_k = D_{k,m} \frac{\nabla w_k}{w_k} + D_{k,m} \frac{\nabla M_n}{M_n} + \frac{D_k^T \nabla T}{\rho w_k T} - z_k \mu_{k,m} E \quad (16)$$

$D_{k,m}$ denotes the average diffusion coefficient, and $\mu_{k,m}$ is average mobility rate of particles k , and z_k is charges of it. These related parameters are listed in Table 1.

Table 1. Parameters relative to discharge.

Parameters	Expression
$D_{k,m}$	$(1 - w_k) / \sum_{j \neq k}^Q \frac{x_j}{D_{kj}}$
$H_{k,m}$	$\frac{eD_{k,m}}{kT}$
$f(w)$	$\frac{2}{\sqrt{\pi} T_e^{3/2}} \exp\left(-\frac{w}{T_e}\right)$
v_{th}^e	$\sqrt{\frac{8kT_e}{\pi m_e}}$
v_{th}	$\sqrt{\frac{8kT}{\pi M}}$
α_k	$\begin{cases} 1, z_k E \cdot n > 0 \\ 0, z_k E \cdot n < 0 \end{cases}$
v_{en}	$6.6^{-19} \times \frac{(T_e/4 - 0.1)}{(1 + (T_e/4)^{16})} n_0 \sqrt{\frac{8kT_e}{\pi m_e}}$
v_{ei}	$2.9^{-12} n_e \sqrt{23} \log\left(\frac{10^{-6} n_e}{T_e^3}\right)$

Boundary conditions

The electrons arriving at the wall of the discharge channel follow the boundary conditions as Eq. 17 and Eq. 18, which illustrate the flux of electrons and their energy on the wall, respectively (Christou and Jugroot 2015). Where $\sum_p \gamma_p$ ($\Gamma_p \cdot n$) denotes the generated flux of secondary electrons, and $\Gamma_p \cdot n$ represents the heat emission rate:

$$\mathbf{n} \cdot \Gamma_e = \frac{1}{2} v_{th}^e n_e - [\sum_p \gamma_p (\Gamma_p \cdot n) + \Gamma_t \cdot n] \quad (17)$$

$$\mathbf{n} \cdot \Gamma_e = \frac{5}{4} v_{th}^e T_e n_e - [\sum_p \gamma_p \varepsilon_p (\Gamma_p \cdot n) + \varepsilon (\Gamma_t \cdot n)] \quad (18)$$

For the particles expect electrons, the flux on the boundary could be expressed as Eq. 19, where v_{th} denotes the thermal velocity of the ions and listed in Table 1 (Christou and Jugroot 2015):

$$\mathbf{n} \cdot \Gamma_k = \rho w_k \left[\frac{v_{th}}{2} + z_k \alpha_k E \cdot n \right] \quad (19)$$

Performance of the thruster

The performances that are concerning are thrust, special impulse and the anode efficiency. The thrust could be calculated in the method of accumulating the product of axial velocity and the mass flow rate of the ions at the exit, as shown in Eq. 20. Special impulse is defined as the consumption of the propellant per unit impulse generated, which is expressed in Eq. 21. And the efficiency could be presented in Eq. 22:

$$T = \sum v_i^+ \Gamma_i^+ \quad (20)$$

$$I_{sp} = \frac{T}{m_{xe}g} \quad (21)$$

$$\eta = \frac{T \cdot I_{sp}}{2P_d} \cdot g \quad (22)$$

where v_i^+ and Γ_i^+ denote the velocity and the mass flow rate of the ions at the exit, respectively. P_d is the power consumed when the thruster is operation, m_{xe} represents the mass flow rate of the propellant and g is gravitational acceleration constant, which is $9.8 \text{ m}\cdot\text{s}^{-2}$.

NUMERICAL SIMULATION RESULTS IN HALL THRUSTER DISCHARGE CHANNEL

This section presents the results of the numerical simulation in the discharge channel of the two thrusters. The simulations have been carried out both in magnetic shielding and conventional configuration and at discharge voltage of 320 V, anode mass flow of $1.7 \text{ mg}\cdot\text{s}^{-1}$. The initial electron temperature is 2 eV and the density is $1.0 \times 10^{18} \text{ m}^{-3}$. The numerical results demonstrate the plasma parameters in the discharge channel, which are relevant to the performance and erosion.

The numerical results of the discharge channel are shown as follows. The spatial potential distribution along the center line of the discharge channel is shown in Fig. 5. In unshielded configuration, the plasma potential drops rapidly inside the discharge channel at an axial location of $\sim 0.7 z \times L^{-1}$. While in the MS configuration, owing to the continuous magnetic field lines that expand to the anode, the spatial potential is higher at the same position in acceleration region than its unshielded counterpart, so that the drop occurs at an axial location of $\sim 0.85 z \times L^{-1}$.

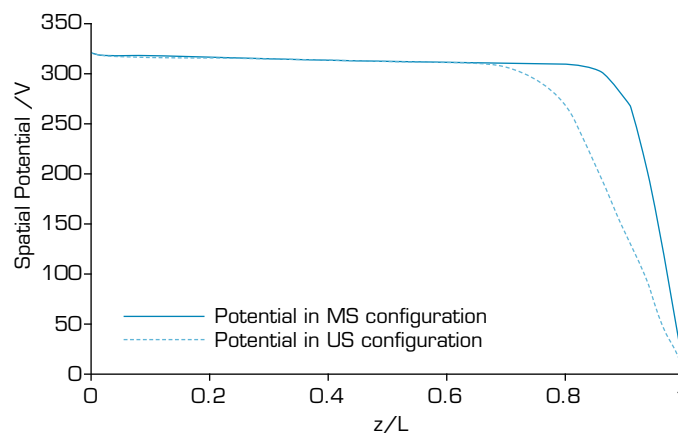


Figure 5. Spatial potential along the center line of the discharge channel.

Figure 6 presents the spatial distribution of the electron density in both configurations. The electron density in the MS configuration in the channel ranges from about $1 \times 10^{17} \cdot \text{m}^{-3}$ to $1.4 \times 10^{18} \cdot \text{m}^{-3}$, a little higher than that in the US configuration, which ranges from $1 \times 10^{17} \cdot \text{m}^{-3}$ to $1.2 \times 10^{18} \cdot \text{m}^{-3}$. And the peak value of the electron density appears at about $z \times L^{-1} = 0.7$ upstream of the exit, while that in conventional configuration is at about $z \times L^{-1} = 0.5$. It indicates that the ionization reaction in MS configuration occurs nearer the exit, which brings in a longer ionization region in the discharge channel.

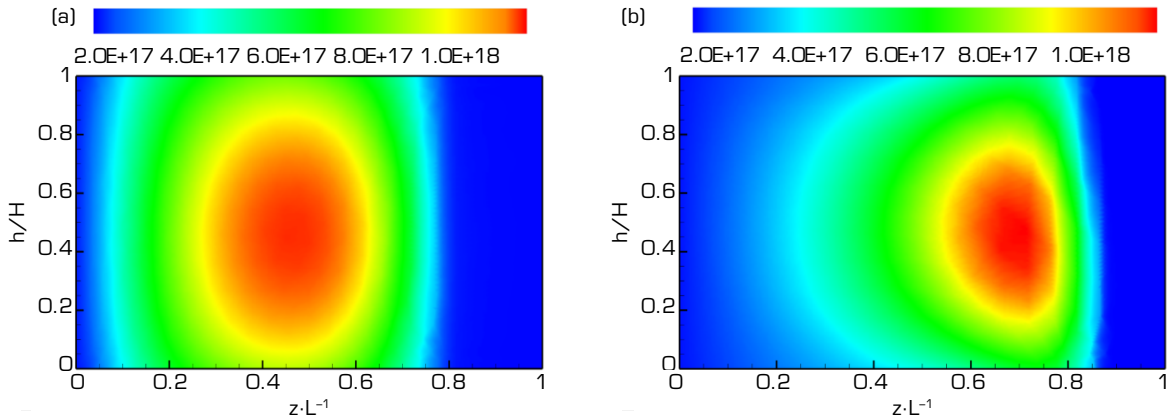


Figure 6. Electron density in the discharge channel of LHT-60 and LHT-60M (m^{-3}). (a) Conventional; (b) Magnetic shielding.

Figures 7 and 8 demonstrate the distribution of the electron temperature in the two configurations. Compared with the conventional configuration, in which the electron temperature remains at about 5 V near the anode and raises quickly to about 27 V at an axial location of $\sim 0.83 z \times L^{-1}$, the T_e in US configuration keeps low along the channel, and reaches its peak value at about $0.9 z \times L^{-1}$. The results also accord with the theory denoted in section “Magnetic design”. The peak value of T_e in MS configuration is also higher than its unshielded counterpart, which can be attributed to the reason as follows:

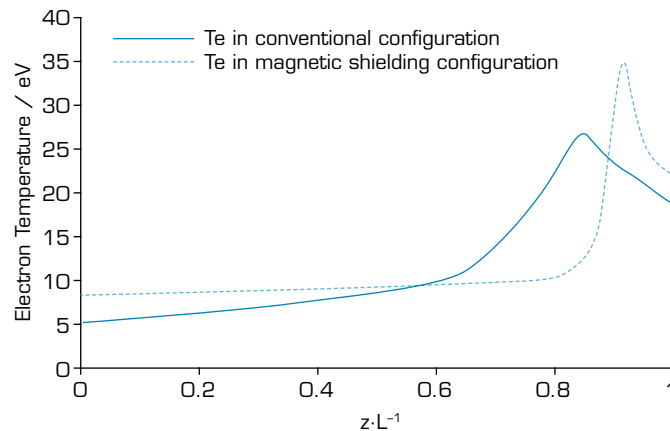


Figure 7. Electron temperature along the center line.

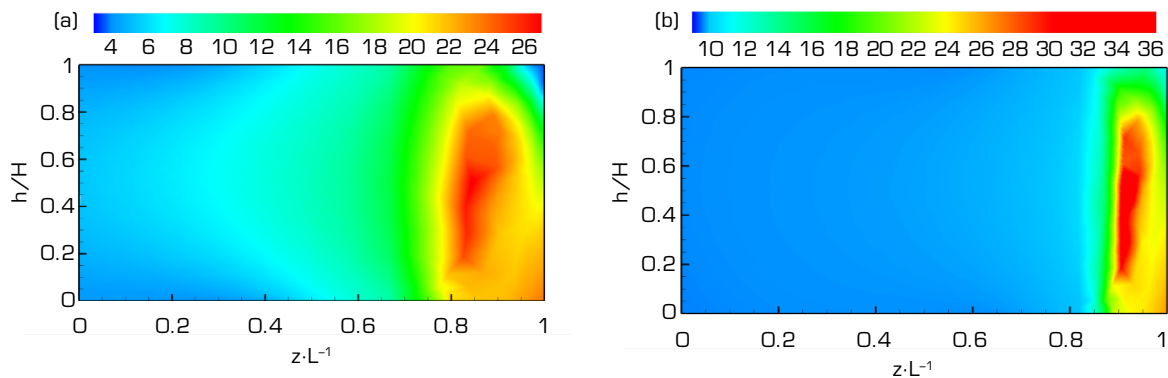


Figure 8. Electron temperature in the discharge channel of LHT-60 and LHT-60M (eV).
(a) Conventional, (b) Magnetic shielding .

Since the electric field intensity in the acceleration region of the discharge channel is larger in MS case, the electrons could capture more energy in this region with little collision and the electron temperature rises continuously to the peak value. Then the electrons participate in the ionization and excitation reaction, where the energy would be consumed by collision with neutral atoms. Meanwhile, in the US configuration, the original electrons are accelerated by a relative weak electric field, and then decelerated in the course of collision with the neutral atoms. Thereby, the distribution of the electron temperature presents a different profile.

EXPERIMENTAL RESULTS AND DISCUSSION

Experiment equipment

The experiment was carried out in a large vacuum facility designed for electric Hall thruster, as shown in Fig. 9. The size of the vacuum chamber is $\Phi 5 \times 10$ m, which could provide a base pressure of 1×10^{-4} Pa with the Hall thruster full power flow rates. As shown in Fig. 10, the thruster is mounted with thrust stand inside the vacuum facility and along the centerline of the chamber near the end to ensure the plume extending completely. The Hall thruster operated at the discharge voltage of 320 V and anode flow rates of $1.7 \text{ mg}\cdot\text{s}^{-1}$.



Figure 9. The vacuum facility for the experiment.

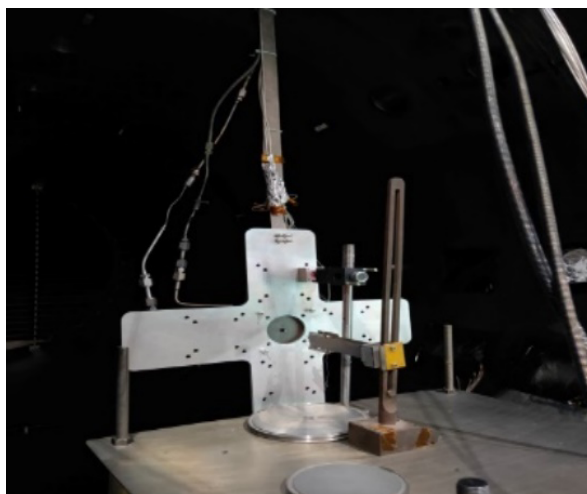


Figure 10. Experiment with thrust stand.

Performances of the thrusters

To validate the applicability of the magnetic shielding configuration on the low-power Hall thruster, the experiments were carried out in the LHT-60 and LHT-60M. The performances, such as thrust, special impulse and efficiency under different discharge voltage were tested, as well as those versus anode mass flows with fixed discharge voltage.

As shown in Fig. 11, the discharge current increases with the rising of the discharge voltage. Current in magnetic shielding configuration is a little higher than that in conventional configuration.

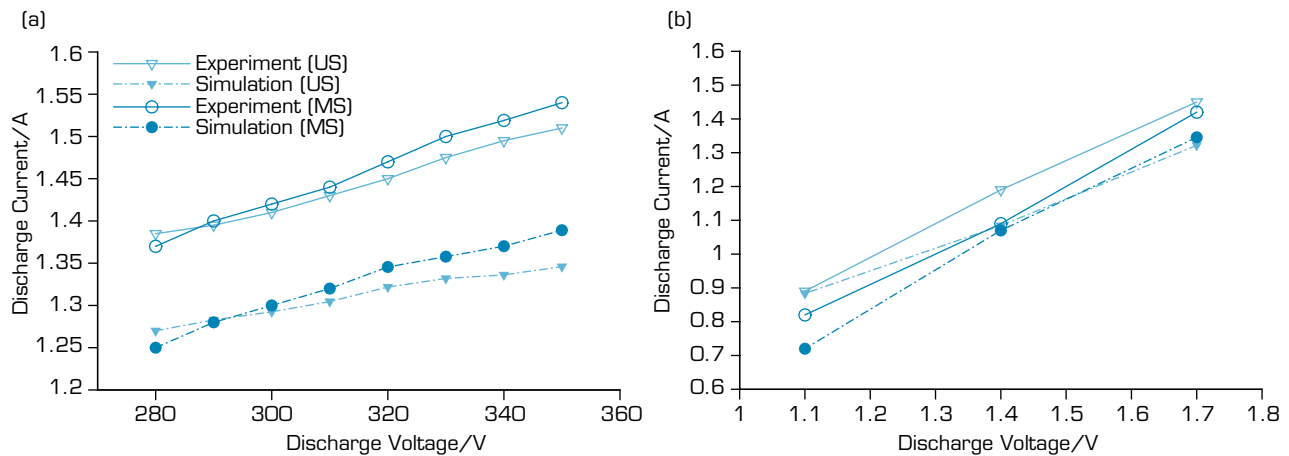


Figure 11. Discharge current of LHT-60 and LHT-60M with (a) fixed anode mass flow and (b) fixed discharge voltage.

The thrust versus discharge voltage for the anode mass flow at $1.7 \text{ mg}\cdot\text{s}^{-1}$ and various with different anode mass flow under fixed voltage is shown in Fig. 12. It can be seen that the thrust of the thruster under MS configuration is a little lower than that in US configuration, whether in fixed anode mass flow or in fixed discharge voltage, which coincides with the prediction of the numerical results shown in the dotted lines. The numerical result is lower than the experimental results and the deviation is no more than 10%. This is because the model mainly focuses on the single valence ions, while the multiple valences ions also contribute to the thrust, as well as the residual air in the vacuum chamber participating in the discharge reaction.

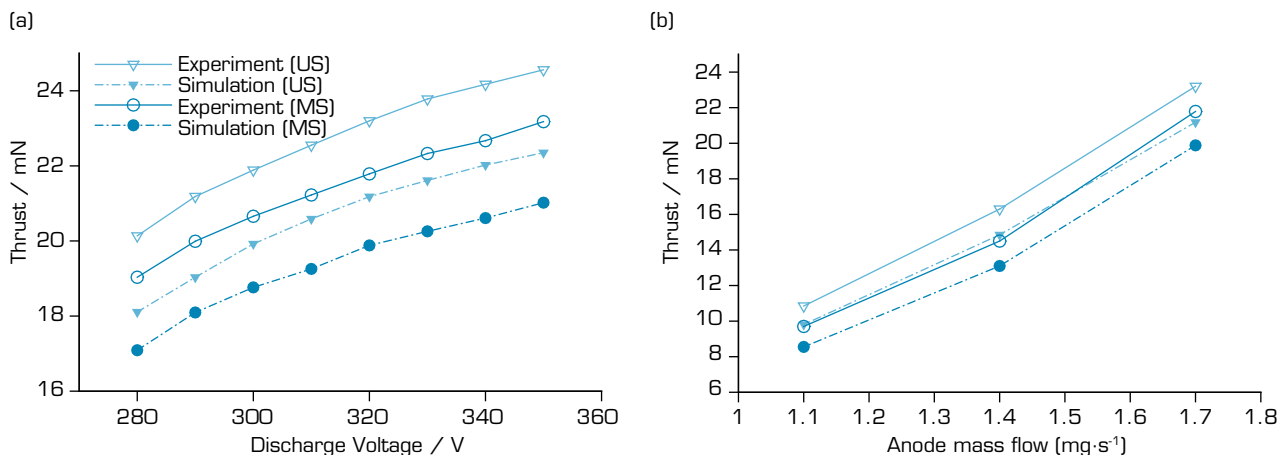


Figure 12. Thrust of LHT-60 and LHT-60M with (a) fixed anode mass flow and (b) fixed discharge voltage.

According to Eq. 21, a similar trend can be found on the special impulse, as shown in Fig. 13. The experimental results range from 1208 to 1474 s in US configuration and 1142 to 1391 s in MS configuration, respectively.

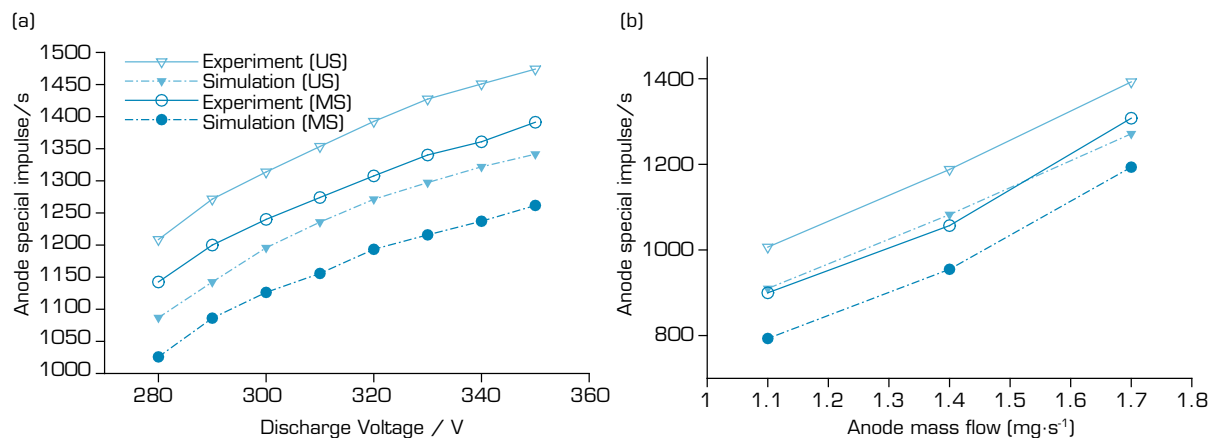


Figure 13. Anode special impulse of LHT-60 and LHT-60M with (a) fixed anode mass flow and (b) fixed discharge voltage.

The results about efficiency versus discharge voltage and anode mass flow are shown in Fig. 14. Similar to the thrust, the efficiency of the MS thruster is lower than that of the US thruster in a whole. The maximum efficiency of the unshielded thruster is 34%, occurring when the discharge voltage is 320 V, the anode mass flow is 1.7 mg·s⁻¹. As for the MS, the peak value of the efficiency is about 30%.

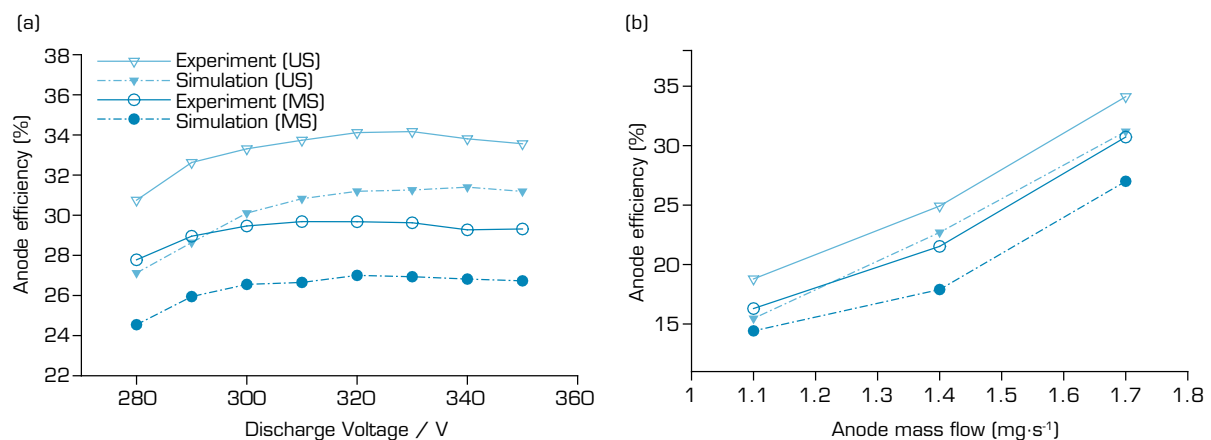


Figure 14. Anode efficiency of LHT-60 and LHT-60M with (a) fixed anode mass flow and (b) fixed discharge voltage.

Erosion of the discharge channel

In order to verify the benefit of the magnetic shielding configuration, an endurance test has been carried out. The LHT-60 has operated in the vacuum chamber for 2000 h up to now, at the discharge voltage 320 V and anode flux 1.7 mg·s⁻¹. The morphology change of the discharge channel in acceleration region was measured every 200 h. Figure 15 shows the Hall thruster operating with Xe at 320 V and 1.7 mg·s⁻¹.

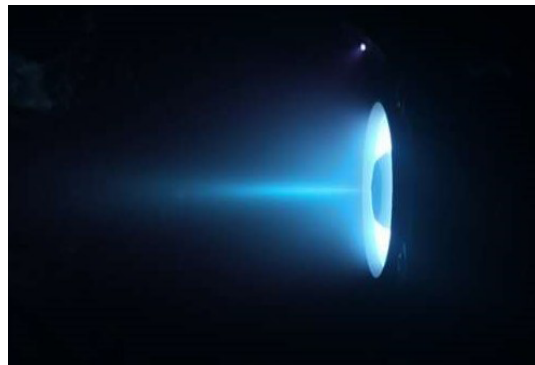


Figure 15. LHT-60M operating with Xe at 320 V and 1.7 mg·s⁻¹.

The erosion mainly happens in the area adjacent exit of the channel, the so-called acceleration region. Therefore, the erosion test focuses on the variation of the appearance in this part. The erosion can be obtained by measuring the position of the surface of the wall through three-dimensional profilometer in every 200 h. The largest variation in each test is adopted to represent the erosion during the past period.

Figure 16 illustrates the tendency of the erosion rate during the whole experiment. On the hall, the erosion rate decreases with the processing of the experiment. In the first 200 h of the test, the erosion rate is about $2.5 \mu\text{m}\cdot\text{h}^{-1}$ and, as the test proceeds, the erosion rate decreased below $1.1 \mu\text{m}\cdot\text{h}^{-1}$ after 1000 h. In the last 600 h, the erosion rate is lower than $0.2 \mu\text{m}\cdot\text{h}^{-1}$. In general, the erosion rate of a SPT-type of the low-power Hall thruster is larger than $5 \mu\text{m}\cdot\text{h}^{-1}$ (Mikellides *et al.* 2014). In contrast, even the largest erosion rate in the LHT-60M is lower than half of that. The experimental results manifest the effectiveness of the magnetic configuration applied on low-power Hall thruster.

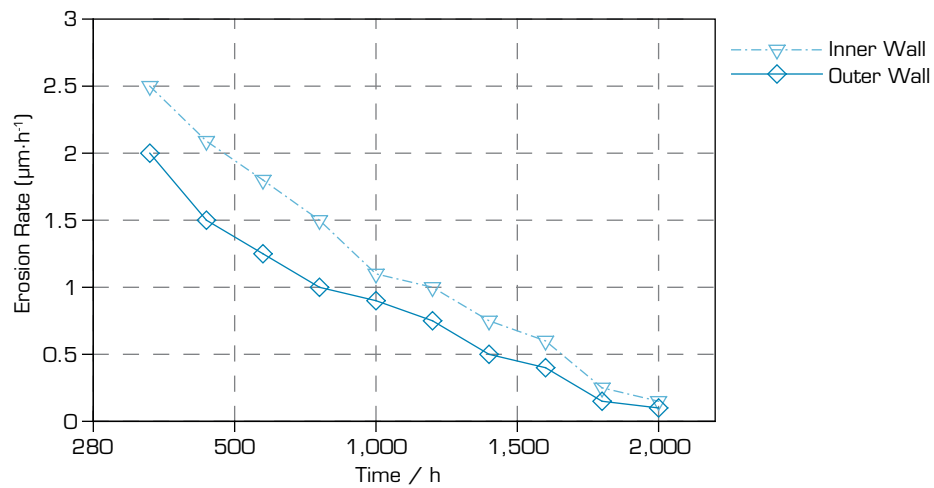


Figure 16. LHT-60M erosion rate through 2000 h test.

Figure 17 shows the average erosion rate in the whole span of the experiment and the erosion rate in last 200 h along the wall, from which it is possible to find that the erosion mainly appears in the region $\sim 25\% z \times L^{-1}$ to the exit. In the last 200 h, the erosion rate decreased below $0.2 \mu\text{m}\cdot\text{h}^{-1}$, which means that the residual lifetime of the thruster is still considerable.

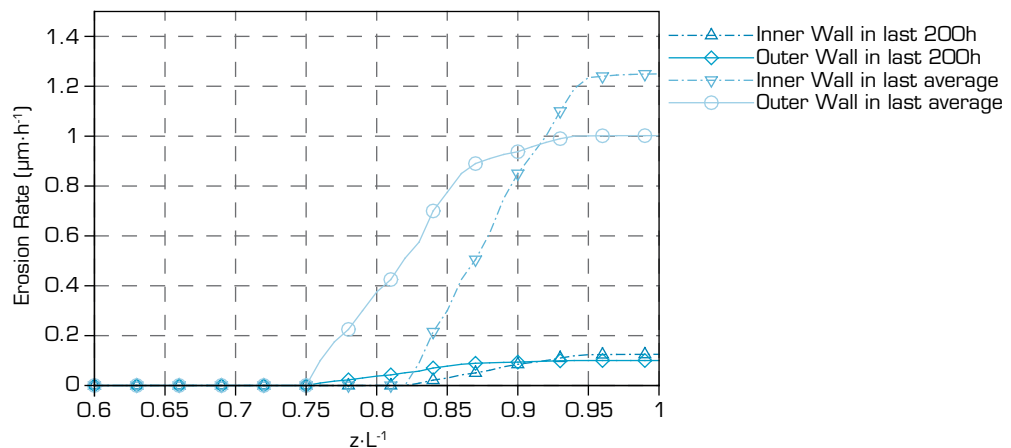


Figure 17. LHT-60M erosion rate along the discharge channel.

CONCLUSIONS

In this paper, both numerical and experimental methods were performed to investigate the effects of the magnetic shielding configuration on the discharge characteristics of the 60-mm diameter Hall thruster. The spatial potential, electron temperature and electron density in discharge channel were compared in two different magnetic topologies. The experimental on performance were also carried out in various conditions. A 2000 h lifetime test was also carried out to validate the effectiveness of the magnetic shielding configuration adopted in low-power Hall thruster.

The results show that the peak value of the electron temperature along the discharge channel and the potential drop occurs much closer to the exit than that in unshielded configuration. For the performance, the anode efficiency in MS configuration is slightly lower than that in US configuration, and the maximum value is 29.7 and 34% in shielded and unshielded configuration, respectively, corresponding to thrust of 21.7 and 23.2 mN. For the lifetime test, the average erosion rate at the exit in 2000 h is about $1 \mu\text{m}\cdot\text{h}^{-1}$, and decreased below $0.2 \mu\text{m}\cdot\text{h}^{-1}$ in last 200 h. It indicates that the partial magnetic shielding configuration is effective. The slight decrease of the performance brought by magnetic configuration could be acceptable in order to prolong the operating lifetime of the thruster. The results demonstrate the effectiveness and benefit of magnetic shielding configuration being applied on the low-power Hall thruster.

AUTHORS' CONTRIBUTION

Conceptualization: Guo W; **Methodology:** Guo W and Gao J; **Investigation:** Guo W and Sun M-m; **Writing – Original Draft:** Guo W; **Writing – Review and Editing:** Gu Z; **Funding Acquisition:** Guo N; **Resources:** Gao J and Guo N; **Supervision:** Gu Z.

DATA AVAILABILITY STATEMENT

The data will be available upon request.

FUNDING

National Natural Science Foundation of China
[<https://doi.org/10.13039/501100001809>]
Grant No. 61901204

ACKNOWLEDGEMENTS

The authors are thankful to Science and Technology on Vacuum Technology and Physics Laboratory for providing the equipment.

REFERENCES

Ahedo E, Martinez P, Martinez-Sanchez M (2000) Steady and linearly-unsteady analysis of a Hall thruster with an internal sonic point. Paper presented 36th AIAA/ASME/SAE/ASEE Joint Propulsion Conference and Exhibit. AIAA; Las Vegas, Nevada, United States. <https://doi.org/10.2514/6.2000-3655>

Book DL (1987) NRL Plasma Formulary. Naval Research Laboratory. Washington: Naval Research Laboratory (U.S.). <https://doi.org/10.21236/ADA247840>

- Christou AG, Jugroot M (2015). Modeling of an electric propulsion system: Towards a hybrid system. Paper presented 45th AIAA Plasmadynamics and Lasers Conference. AIAA; Atlanta, Georgia, United States. <https://doi.org/10.2514/6.2014-2233>
- Christou A, Jugroot M (2017) Investigating a two-stage electric space propulsion system: Simulation of plasma dynamics. *Vacuum* 141:22-31. <https://doi.org/10.1016/j.vacuum.2017.03.003>
- Conversano RW, Goebel DM, Hofer RR, Matlock TS, Wirz RE (2015) Development and initial testing of a magnetically shielded miniature Hall thruster. *IEEE Trans Plasma Sci* 43(1):103-117. <https://doi.org/10.1109/TPS.2014.2321107>
- Jacobson D, Jankovsky R (1998) Test results of a 200W class Hall thruster. Paper presented 34th AIAA/ASME/SAE/ASEE Joint Propulsion Conference and Exhibit. AIAA; Cleveland, Ohio, United States. <https://doi.org/10.2514/6.1998-3792>
- Duan P, Liu G, Bian X, Chen L, Yin Y, Cao A (2016) Effect of the Discharge Voltage on the Performance of the Hall thruster. *Plasma Sci Technol* 18(4):382-387. <https://doi.org/10.1088/1009-0630/18/4/09>
- Escobar D, Ahedo E (2015) Global Stability Analysis of Azimuthal Oscillations in Hall thrusters. *IEEE Trans Plasma Sci* 43(1):149-157. <https://doi.org/10.1109/TPS.2014.2367913>
- Goebel DM, Katz I (2008) *Fundamentals of Electric Propulsion: Ion and Hall thrusters*. Hoboken: John Wiley & Sons. <https://doi.org/10.1002/9780470436448>
- Grimaud L, Mazouffre S (2017). Conducting wall Hall thrusters in magnetic shielding and standard configurations. *J Appl Phys* 122(3):033305. <https://doi.org/10.1063/1.4995285>
- Grimaud L, Mazouffre S (2018) Performance comparison between standard and magnetically shielded 200 W Hall thrusters with BN-SiO₂ and graphite channel walls. *Vacuum* 155:514-523. <https://doi.org/10.1016/j.vacuum.2018.06.056>
- Hargus Junior WA, Charles CS (2003) Near Exit Plane Velocity Field of 200 W Hall thruster. Paper presented 39th AIAA/ASME/SAE/ASEE Joint Propulsion Conference and Exhibit. AIAA; Huntsville, Alabama, United States. <https://doi.org/10.2514/6.2003-5154>
- Hruby V, Monheiser J, Pote B, Rostler P, Kolencik J, Freeman C (1999), Development of low power Hall thrusters. Paper presented 30th Plasmadynamic and Lasers Conference. AIAA; Norfolk, Virginia, United States. <https://doi.org/10.2514/6.1999-3534>
- Katz I, Mikellides IG, Goebel DM (2004) Model of the Plasma Potential Distribution in the Plume of a Hollow Cathode. Paper presented 40th AIAA/ASME/SAE/ASEE Joint Propulsion Conference and Exhibit. AIAA; Fort Lauderdale, Florida, United States. <https://doi.org/10.2514/6.2004-4108>
- Mikellides I, Katz I, Hofer R, Goebel D, Grys K, Mathers A (2010). Magnetic Shielding of the Acceleration Channel Walls in a Long-Life Hall thruster. Paper presented 46th AIAA/ASME/SAE/ASEE Joint Propulsion Conference and Exhibit. AIAA; Nashville, Tennessee, United States. <https://doi.org/10.2514/6.2010-6942>
- Mikellides IG, Katz I, Hofer RR, Goebel DM, Grys K, Mathers A (2011) Magnetic shielding of the channel walls in a Hall plasma accelerator. *Phys Plasmas* 18:033501. <https://doi.org/10.1063/1.3551583>
- Mikellides I, Katz I, Hofer R (2013) Design of a Laboratory Hall thruster with Magnetically Shielded Channel Walls, Phase I: Numerical Simulations. Paper presented 47th AIAA/ASME/SAE/ASEE Joint Propulsion Conference & Exhibit. AIAA; San Diego, California, United States. <https://arc.aiaa.org/doi/10.2514/6.2011-5809>
- Mikellides IG, Katz I, Hofer RR, Goebel DM (2014) Magnetic shielding of a laboratory Hall thruster. I. Theory and validation. *J Appl Phys* 115(4):043303. <https://doi.org/10.1063/1.4862313>
- Szabo JJ, Tedrake R, Metivier E, Paintal S, Taillefer Z (2017) characterization of a one hundred watt, long lifetime hall effect thruster for small spacecraft. Paper presented at 53rd AIAA/SAE/ASEE Joint Propulsion Conference. AIAA; Atlanta, Georgia, United States. <https://doi.org/10.2514/6.2017-4728>